Design, synthesis, *in vitro*, and *in silico* evaluations of kojic acid derivatives linked to amino pyridine moiety as potent tyrosinase inhibitors

Davood Rezapour Niri [a], Mohammad Hosein Sayahi [b], Somayeh Behrouz [a],
Ali Moazzam [c], Fatemeh Rasekh [g], Nader Tanideh [d], Cambyz Irajie [e],
Mohammad Seif Nezhad [d], Bagher Larijani [c], Aida Iraji [d,f,*], Mohammad Mahdavi [c,**]

[a] Medicinal Chemistry Research Laboratory, Department of Chemistry, Shiraz University of Technology, Shiraz, Iran
[b] Department of Chemistry, Payame Noor University (PNU), Tehran, Iran
[c] Endocrinology and Metabolism Research Center, Endocrinology and Metabolism Clinical Sciences Institute, Tehran, Iran
[d] Stem Cells Technology Research Center, Shiraz University of Medical Sciences, Shiraz, Iran
[e] Department of Medical Biotechnology, School of Advanced Medical Sciences and Technologies, Shiraz University of Medical Sciences, Shiraz, Iran
[f] Research Center for Traditional Medicine and History of Medicine, Department of Persian Medicine, School of Medicine, Shiraz University of Medical Sciences, Shiraz, Iran
[g] Department of Biology, Payame Noor University (PNU), Tehran, Iran

A R T I C L E   I N F O

A B S T R A C T

In the present study, novel series of kojic acid derivatives conjugated to amino pyridine moiety were designed and synthesized to explore their inhibitory activity against tyrosinase. To this end, the structure of all derivatives was characterized by ^{1}H NMR, ^{13}C NMR, FT-IR, and elemental analysis. Next, all derivatives were evaluated against tyrosinase compared to the kojic acid as positive control and exhibited different inhibitory potencies. Furthermore, the antioxidant potential of all derivatives was determined. The kinetic analysis of the most active agent revealed that 3-hydroxy-6-(hydroxymethyl)-2-((3-nitrophenyl)(pyridin-2-ylamino)methyl)-4H-pyran-4-one (**4h**) binds to the enzyme in the uncompetitive mode of action. The docking analysis and molecular dynamic simulations showed considerable binding affinity and significant interactions with tyrosinase enzyme to target the melanogenesis pathway, proposing them as potent candidates to control hyperpigmentation in the future.

1. Introduction

Melanin produced by melanocytes is responsible for the pigmentation of skin, hair, and eyes and plays an important role in protecting human skin from the destructive effect of UV radiation and oxidative stress []. However, excessive melanin synthesis can cause abnormal pigmentation, age spots, freckles, and induce skin diseases as well as malignant melanoma [1]. Tyrosinase (EC 1.14.18.1,

---

* Corresponding author. Stem Cells Technology Research Center, Shiraz University of Medical Sciences, Shiraz, Iran. Research Center for Traditional Medicine and History of Medicine, Department of Persian Medicine, School of Medicine, Shiraz University of Medical Sciences, Shiraz, Iran.
** Corresponding author. Endocrinology and Metabolism Clinical Sciences Institute, Tehran University of Medical Sciences, Tehran, Iran.
E-mail addresses: aida.iraji@gmail.com, iraji@sums.ac.ir (A. Iraji), momahdavi@sina.tums.ac.ir (M. Mahdavi).

TYR) is metalloenzyme with six histidine residues and two conserved copper ions in its active site, which is essential for the catalytic activity of tyrosinase [2]. Tyrosinase hydroxylates L-tyrosine to L-dihydroxyphenylalanine (L-DOPA), which is then oxidized to form dopaquinone, and subsequently undergoes a series of reactions to form melanin [3,4]. Also, the undesirable tyrosinase phenomena in browning fruits, vegetables, and seafood resulted in around 50 % of the market's economic losses [,5]. Tyrosinase inhibitors are now commercially available from natural or synthetic sources [6]. Various potent tyrosinase inhibitors have recently been developed, including chalcone [7], thiazole-oxadiazol [8], benzylidenethiazol [9], thioquinoline [10], tetralone [11], benzothiazepine [12], 2-phenylchromone [13,14], flavone-based hydrazone [15], 2-arylchrome-4-thione [16], and aurone [17] (Fig. 1).

Kojic acid and arbutin are potent tyrosinase inhibitors with poor penetration and potency [18,19]. As a result, finding inhibitors with high activity and low side effects has practical value in preventing or even treating hyperpigmentation. Kojic acid (compound **A**, Fig. 2) is a potent tyrosinase inhibitor with a UV protector and skin-whitening potencies. Also, some reports about its collagen synthesis enhancer make it an ideal agent in the pharmaceutical and cosmetic industries [20,21]. However, it demonstrated various side effects, including skin irritation, toxicity, and instability during storage, thus reducing its use in products. Many kojic acid derivatives have been produced in recent years to overcome these drawbacks. It has been reported that compound **B** with two coupled kojic acid ((E)-6, 6'-(ethene-1,2-diyl)bis(3-hydroxy-4H-pyran-4-one); Fig. 2) was about eight times more potent with $IC_{50} = 3.63$ μM than that of kojic acid ($IC_{50} = 30.61$ μM) [22]. In another work, kojic acid-triazole-based structure (4-((1-((5-hydroxy-4-oxo-4H-pyran-2-yl)meth-yl)-1H-1,2,3-triazol-4-yl)methoxy)-2H-chromen-2-one; compound **C**, Fig. 2) was evaluated as a tyrosinase inhibitor, and all derivatives exhibited IC_{50} values ≤ 3.75 μM compared to kojic acid ($IC_{50} = 9.28$ μM). The importance of *ortho*-methoxy and *para*-acetyl group substitutions on this scaffold was shown by structure-activity relationship (SAR) analysis. The kinetic studies of the most potent derivative indicated mixed-type inhibition [19]. In another study, kojic acid linked to substituted thio-quinazolines (2-(((5-hydrox-y-4-oxo-4H-pyran-2-yl)methyl)thio)-3-(pyridin-2-ylmethyl)quinazolin-4(3H)-one; compound **D**, Fig. 2) demonstrated IC_{50} values in the range of 0.46–5.32 μM. The most potent agent showed the important role of kojic acid moiety to participate in two H-bond interactions with critical His259 and His85 coordinated with CuA and CuB [23].

Pyridine is a common scaffold present in several pharmaceuticals and natural products with a wide range of activities as anticancer [24], anti-inflammatory [25], antimicrobial [26], and antidiabetes [27] agent. Also, the anti-melanogenesis role of pyridine was confirmed in different studies as a critical scaffold to fit in the binding site of tyrosinase properly and exhibited different interactions, including H-bound, hydrophobic, hydrophilic, and metal chelation potentials [,28,29]. In this context, compounds **D** and **E** represented improved tyrosinase inhibition and induced inhibitory activities against melanin formation [30].

Also, antioxidant activity are important pharmacological properties possessing antiaging, antimutagenicity, anticarcinogenic, and skin-whitening activities. Studies of antioxidants are coming to the front of researchers for application use in foods or medicinal [31–33].

In this regard, a series of kojic acids linked to amine pyridine were synthesized, and their tyrosinase inhibitory activities were examined using mushroom tyrosinase. The mode of tyrosinase inhibition by the most active agent was determined by kinetic studies. Afterward, the molecular dynamics simulations of the most potent derivative were examined. In addition, the antioxidant effects of these derivatives using DPPH (2,2-diphenyl-1-picrylhydrazyl) were investigated.

IC_{50} = 50 nM

IC_{50} = 0.025 μM

IC_{50} = 0.093 ± 0.003 μg/ml

IC_{50} = 1.04 ± 0.05 μM
No toxicity up to 20 μM at 72 h

IC_{50} = 7.12 ± 0.32 μM

IC_{50} = 1.12 ± 0.04 μM

IC_{50} = 4.64 μM

IC_{50} = 1.21 μM

IC_{50} = 25.75±0.19 μM
No toxicity up to 32 μM
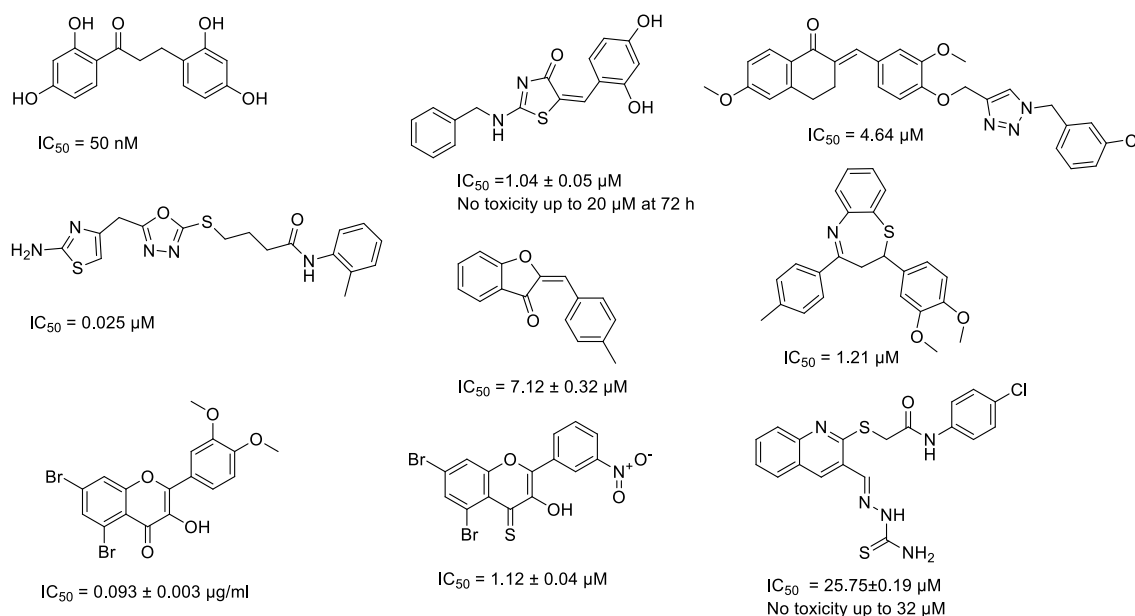
Fig. 1. Recently reported highly potent tyrosinase inhibitors.
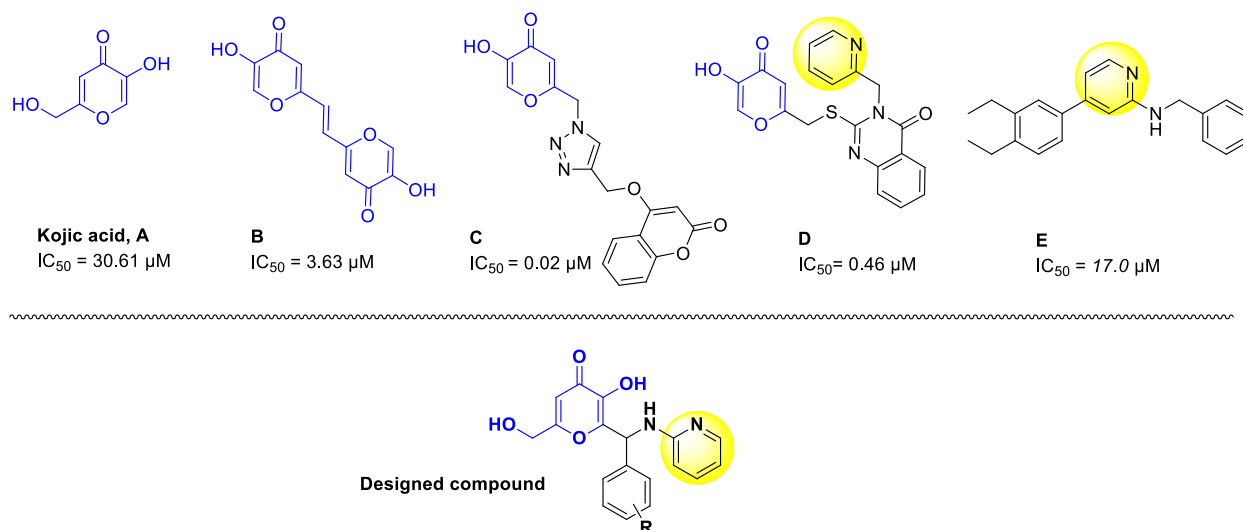
Fig. 2. Chemical structure of representative tyrosinase inhibitors and newly designed compounds.

2. Results and discussion

2.1. Chemistry

The one-pot synthesis procedures of **4a-m** derivatives were exhibited in Scheme 1. A mixture of kojic acid (compound **1**, 1 mmol) and 2-amino pyridine (compound **2**, 1 mmol), and benzaldehyde derivatives (**3**, 1.3 mmol) under neat conditions were stirred at 80 °C for 4 h. The progress of the reaction was monitored by thin-layer chromatography. After completion of the reaction, ethyl acetate was added to the reaction mixture; the precipitated product was filtered and dried to give the corresponding final products **4a-m**. The reaction mechanism contains the formation of an imine structure between aldehyde and 2-amino pyridine. Then nucleophilic attack from enol group of kojic acid to mine bond and consequently formation desired products.

All compounds were fully characterized by ^{1}H NMR, ^{13}C NMR, FT-IR, and elemental analysis. Investigation of ^{1}H NMR spectrum of **4a** indicated that a singlet peak at 9.23 ppm related to OH enol, singlet peak at 7.96 ppm related to C–H of the kojic acid ring, multiple peaks at 7.44–7.25 ppm related to the aromatic ring, doublet of doublet peaks at 6.72 and 6.67 ppm related to pyridine ring that shieled with electron donating group, triplet peak at 6.54 ppm related to NH, triplet peak at 6.30 ppm related to C–H aliphatic, triplet peak at 5.63 ppm related to OH, quartet-doublet peak at 4.28 ppm related to enantiotopic O–CH$_2$. ^{13}C NMR spectrum of **4a** confirmed the structure, peak at 174.23 ppm related to the carbon of carbonyl (C=O), peak at 167.83 ppm related to the carbon of Cq-O in kojic acid ring, peak at 157.85 ppm related to the carbon of Cq –OH bond, peak at 149.96 ppm related to the carbon of Cq –N bond, peak at 147.80 ppm related to the carbon of Cq –N bond

Between 141.42 and 109.38 ppm related to aromatic carbon, peak at 59.94 ppm related to related to aliphatic carbon (CH$_2$) of C–O bond, peak at 50.60 ppm related to aliphatic carbon (CH$_2$) of C–N bond. Investigation of the IR (KBr) spectrum of **4a** indicated that the peak at 3265 cm^{-1} was related to O–H group, the peak at 1632 cm^{-1} was related to the carbonyl group, the peak at 1550 cm^{-1} was related to the aromatic region, the peak at 1361 cm^{-1} related to C–N bond, peak at 1231 cm^{-1} related to C–O bond.

2.2. SAR based on tyrosinase inhibition & docking studies

The inhibitory activities of kojic acid derivatives linked to amine pyridine moiety were evaluated against mushroom tyrosinase using kojic acid as the positive control. All derivatives dose-dependently inhibited tyrosinase and the results of *in vitro* and *in silico*
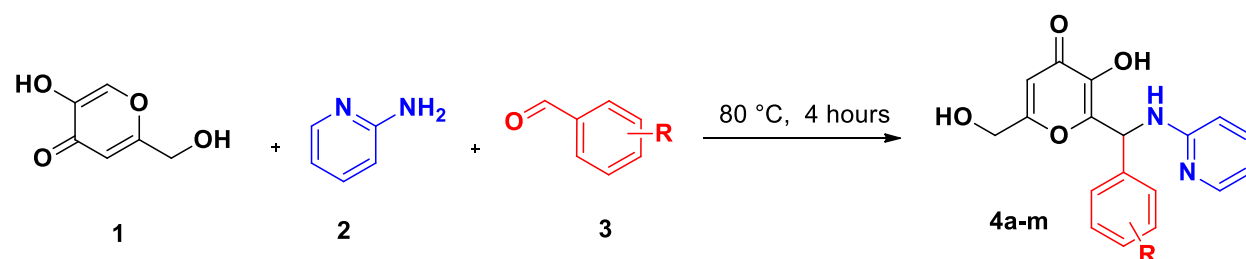
Scheme 1. Synthesis of compounds **4a-m**.

studies are summarized in Table 1.

Compound **4a** with no substitution at the R position exhibited weak potencies with 29.14 % inhibition at 50 μM with docking score = −5.095 kcal/mol. The results of the *in silico* study revealed that the hydroxyl group of the kojic moiety formed a hydrogen bond with His279, in addition to engaging in a pi-cation interaction with Arg268. Conversely, compound **4a** exhibited favorable interactions with Asn260, Val283, and Met280. Despite these interactions, it is noteworthy that the critical copper ions were not effectively coordinated, which subsequently provides a rationale for the observed limited potency of **4a**.

The fluorine substitution at the *ortho* positions of the phenyl ring (compound **4b**) resulted in a considerable rise in the enzyme inhibitory activity with an IC_{50} value of 28.18 μM (docking score = −5.814 kcal/mol). The kojic moiety demonstrated dual interactions, engaging with both copper ions and forming a hydrogen bond with Ser282. An additional hydrogen bond interaction was observed with His85 on a different molecule region, thereby establishing a correlated relationship between these interactions and potency.

Contrastingly, the *meta* fluorine substitution (compound **4c**) did not yield enhancements compared to the **4b** derivative. The introduction of a 3-F substituent led to a molecular rotation that disrupted the interactions of the kojic moiety with pivotal residues and copper ions. Instead, it interacted with Gly281 through a hydrogen bond and His85 through a pi-pi stacking interaction.

Assessment of the other halogens also exhibited interesting results so that compound **4d** with 2-Cl substitution recorded an IC_{50} value of 22.38 μM, and replacing the position from *ortho* to *meta* decreased the potency so that compound **4e** (R = 3-Cl) recorded an IC_{50} value of 44.67 μM. A molecular docking study effectively predicts a higher potency for the 2-Cl substitution (docking score = −6.106 kcal/mol) than R = 3-Cl (−5.249 kcal/mol). The kojic moiety of **4d** exhibited metal coordination with both copper ions, pi-pi stacking with His263, and hydrogen bonding interactions with His279. Additionally, the chlorine moiety demonstrated a halogen bond interaction with Gly281. However, the substituted pyridine group did not interact with any residue in the active site, although the kojic moiety consistently displayed interactions with copper ions and Met280.

The same trend was seen in bromide substitutions, so 2-Br (compound **4f**, IC_{50} = 23.44 μM) exhibited better activity than entry **4g**. The bromine substitution effectively blocked the active site by occupying the interior surface grooves, similar to the potent derivative kojic moiety. It displayed two metal coordination interactions with Cu ions and formed a hydrogen bond with Met280. Another interaction was observed with His85 and the pyridine group. However, 3-bromine (**4g**) was not successful in participating in both interactions with Cu ions, which led to a reduction in its activity.

Derivative **4h** bearing the 3-NO$_2$ group with strong electron-withdrawing potencies is known as the most potent derivative in this group with an IC_{50} value of 20.42 μM, such modification significantly boosted the docking score (−6.303). The kojic moiety exhibited crucial interactions, forming coordination bonds with two Cu^{2+} ions and hydrogen bonds with His279. It also engaged in pi-pi stacking interactions with His263. Furthermore, the nitro group recorded hydrogen bond interactions with Val83 and Val85.

Unexpectedly, introducing a methoxy group as an electron-donating group into **4h** resulted in **4i**, which exhibited reduced potency (IC_{50} = 30.90 μM). This derivative showed two interactions with Cu^{2+}, a hydrogen bond with His279, and a pi-pi stacking interaction

Table 1
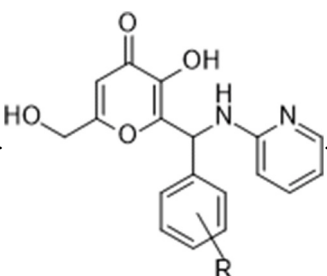
Tyrosinase inhibitory activities of **4a-m**.

Compound	R	% inhibition at 50 μM	IC_{50} (μM) ± RSD[b]	Docking energy
4a	H	29.14 ± 2.86	–	−5.095
4b	2-F	59.42 ± 5.71	28.18 ± 3.63	−5.814
4c	3-F	28.47 ± 1.59	–	−5.192
4d	2-Cl	60.35 ± 1.43	22.38 ± 3.34	−6.106
4e	3-Cl	50.57 ± 2.65	44.67 ± 3.59	−5.249
4f	2-Br	60.85 ± 4.29	23.44 ± 4.19	−6.344
4g	3-Br	33.71 ± 4.88	–	−5.608
4h	3-NO$_2$	74.85 ± 4.26	20.42 ± 2.15	−6.303
4i	3-NO$_2$-4-OMe	56.57 ± 3.84	30.90 ± 4.13	−6.160
4j	3-Me	16.85 ± 3.14	–	−5.092
4k	4-Me	22.28 ± 4.52	–	−4.243
4l	2-OH-3-OMe	52.07 ± 5.27	37.15 ± 5.42	−6.763
4m	4-Ethoxybenzene	35.42 ± 2.43	–	−5.449
Kojic acid[c]	–		23.64 ± 2.56	

[a]50 % inhibitory concentration (IC_{50}).

[b] Values represent means ± RSD.

[c] Kojic acid as the positive control.

with His263. Additionally, the terminal nitro group exhibited a salt bridge interaction with Arg268. However, it appears that the docking study was not entirely successful in anticipating the slight reduction in potency.

Overall, it can be understood that the presence of the electron-withdrawing group at the R position improved the potencies, and the referable position is *ortho*. It was assumed in these cases, the halogen at the *ortho* position was more favorable compared to *meta* substitutions. Also, chlorine derivatives exhibited better activity than fluorine and bromine counterparts due to their optimum size to occupy the binding pocket of tyrosinase. Evaluations on other derivatives bearing electron-donating groups, **4j** (R = 3-methyl) and **4k** (R = 4-methyl) exhibited just 16.86% and 22.28 % inhibition at 50 μM with IC_{50} values > 50 μM.

Regarding derivatives **4l** and **4m**, multiple substitutions and increased bulkiness appear to favor inhibition among electron-donating groups. However, these modifications did not successfully enhance potency compared to the electron-withdrawing groups. Analysis of molecular docking studies for all derivatives revealed that in the potent analogs, the kojic moiety engaged in interactions with two copper ions, and the OH moiety of kojic exhibited hydrogen bond interactions with essential residues in the binding site, including Met280, His263, and His279. Additionally, the substituted moiety of the pyridine group established at least one interaction with the enzyme's binding site.

2.3. Enzyme kinetic studies

According to Fig. 3, the Lineweaver-Burk plot showed that the K_m and V_{max} gradually decreased with increasing inhibitor concentration, indicating an uncompetitive inhibitor of **4h**.

2.4. Antioxidant activity

The possible role of antioxidants in declining hyperpigmentation was reported in some studies. As a result, the antioxidant properties of all derivatives were evaluated using the DPPH assay. The results of the DPPH assay are presented in Table 2. Compound **4a** exhibited weak antioxidant potential with just 20.86 % inhibition at 200 μM. The substitution of halogen groups did not improve the potencies compared to the unsubstituted derivative, **4a**. The same trend was seen in methyl substitutions on the phenyl ring. Among all derivatives, compound **4i** (R = 3-NO_2-4-MeO) exhibited 64.24 % inhibition at 200 μM (IC_{50} = 120.59 μM) followed by **4h** (R = 3-NO_2) with 37.21 % inhibition at 200 μM.

2.5. Molecular dynamic simulations

To investigate the binding interaction and inspect the stability of tyrosinase in the presence of a potent compound **4h**, molecular dynamics (MD) simulation was performed. The stability of the **4h**-tyrosinase complex was examined by root-mean-square-deviation (RMSD). The RMSD of the system illustrates that 30 ns simulation time is adequate to attain equilibration at temperature 310 K (Fig. 4). The low RMSD curve supports the high stability of the conformation. Initially, the RMSD curve of the tyrosinase-**4h** complex gradually increased, then plateaued at around 1.50 Å after 22 ns of simulation time. The RMSD curve of the tyrosinase-troponin complex also exhibited a plateau at approximately 1.65 Å, while the apoenzyme alone showed an RMSD value of 2 Å. These results indicate the excellent stability of the native ligand and **4h** within the enzyme's active site, highlighting its potency.

Additionally, the RMSF value is defined as the fluctuation of the protein's residues from its average position throughout the simulation, which represents the flexibility of protein structure (Fig. 5). Comparing the RMSF values shows that the secondary structure elements have low RMSF values in the tyrosinase-**4h** complex. In contrast, residues of 60–90 and 320 to 340 without the finite secondary structure fluctuated more than other protein regions.

Generally, it was observed that one end of the compound **4h** (the kojic acid moiety) remains to stick with the two critical copper chelating interactions which coordinated with six important His residues named His61, His85 and His94 as well as His2569, His263, and His296 within the binding site of the enzyme (Fig. 6). At the other side of the molecule, nitro-phenyl participated in pi-pi stack
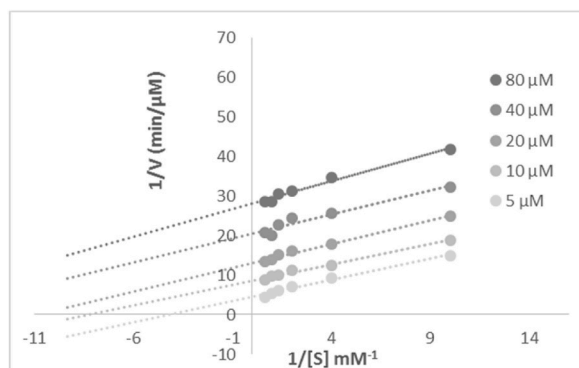
Fig. 3. Kinetic study of inhibitor **4h** against tyrosinase.

Table 2
Antioxidant properties of synthesized compounds using DPPH assay[a].

Compound	% inhibition at 200 μM	IC$_{50}$(μM) ± RSD
4a	20.86 ± 4.41	–
4b	14.09 ± 4.10	–
4c	18.65 ± 3.05	–
4d	19.49 ± 3.98	–
4e	17.21 ± 4.01	–
4f	13.03 ± 2.86	–
4g	18.44 ± 1.54	–
4h	37.27 ± 5.42	–
4i	64.24 ± 3.39	120.59 ± 10.36
4j	17.90 ± 6.77	–
4k	26.96 ± 2.54	–
4l	30.61 ± 5.76	–
4m	23.30 ± 5.17	–
Quercetin [b]	–	18.56 ± 2.19

[a] Data presented here are the mean ± S.E.
[b] Positive control.
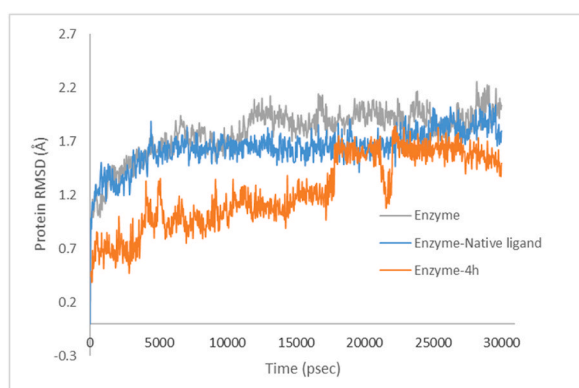
Fig. 4. RMSD plot of the tyrosinase backbone in complexed compound **4h** in the MD simulation time (orange color), RMSD values of tyrosinase with tropolone (blue color), tyrosinase (gray color)
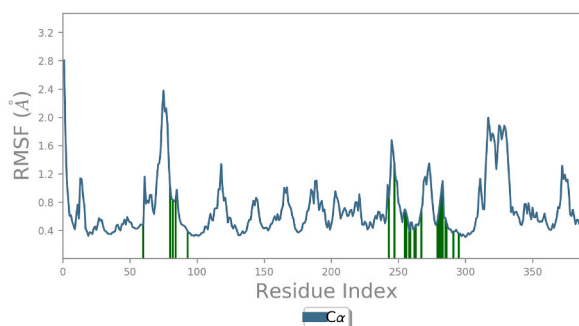
Fig. 5. RMSF plot of the tyrosinase residue in complexed with **4h**.

interaction with His263. Also, the nito group showed pi-cation interaction with Phe264 plus H-bound interaction with Arg268 mediated with water.

Evaluation of tropolone as a native ligand exhibited two critical copper chelating interactions in around 100 % of simulation time, which coordinated with His61, His85 and His94, His259, His263, and His296 within the binding site of the enzyme (Fig. 7).

Overall, the high potency of **4h** was due to the interactions with copper cofactors and critical His residues, which play a significant role in the oxidation of L-tyrosine to L-DOPA and then dopaquinone.
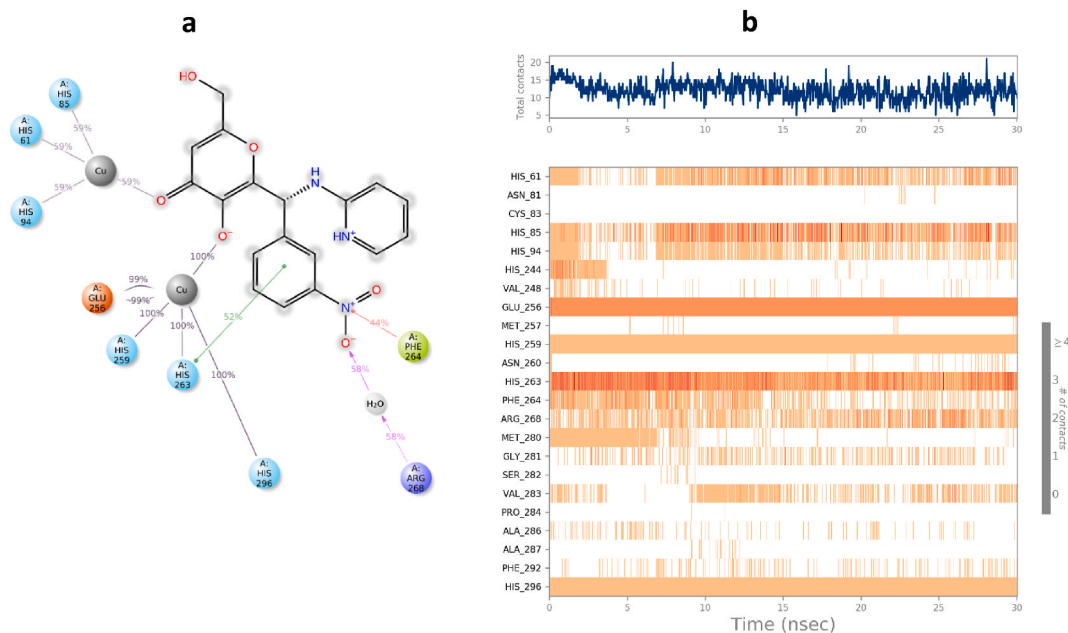
Fig. 6. a) 2D representation of tropolone-residue interactions that occur more than 30.0 % of the simulation time, b) timeline interactions timeline of **4h** with the active site of the enzyme.
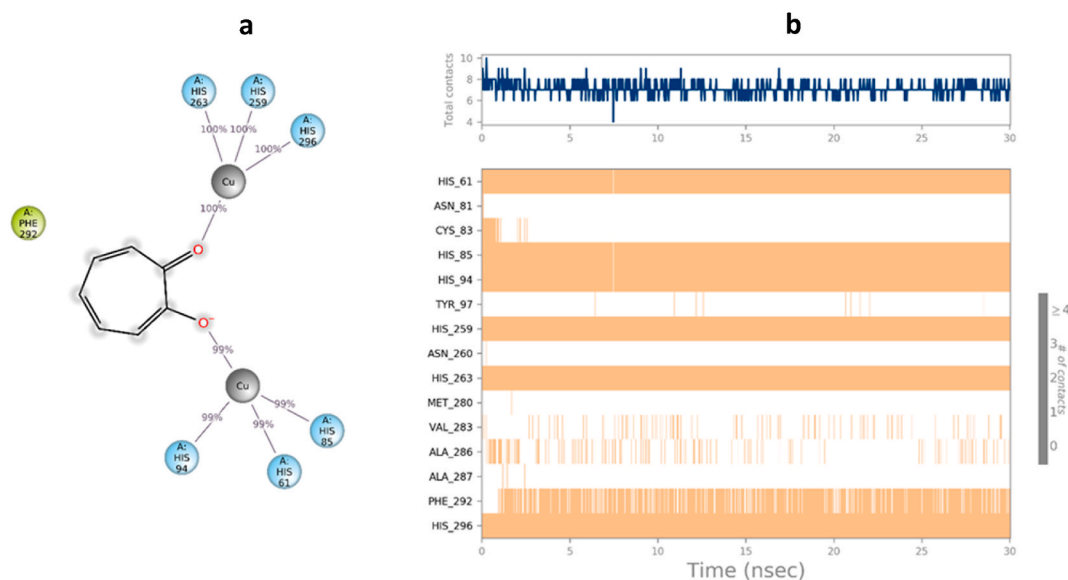
Fig. 7. a) 2D representation of tropolone-residue interactions that occur more than 30.0 % of the simulation time, b) timeline interactions timeline of tropolone with the active site of the enzyme.

3. Conclusion

Due to the significant cosmetic concern posed by abnormal pigmentation and its substantial impact on both quality of life and susceptibility to life-threatening diseases, a pressing demand exists for effective melanogenesis inhibitors. This work reports a method for the synthesis of kojic acid derivatives linked to amine pyridine moiety and the tyrosinase inhibitory potencies of all derivatives were performed. *In vitro* evaluations showed that **4h** derivative was the most potent agent with an IC_{50} value of 20.42 ± 2.15 μM. Furthermore, limited SARs were established for all the synthesized compounds, considering the role of various substituents on the phenyl ring. It was understood that electron-withdrawing groups such as 3-NO$_2$, 2-Cl, 2-F, 2-Br, and 3-Cl were in favor of inhibition compared to electron-donating groups. Afterward, the antioxidant activities of compounds were determined, and particularly

derivative **4i** bearing 3-NO$_2$-4-MeO moiety exhibited the best results. The kinetic studies demonstrated that compound **4h** acts as an uncompetitive inhibitor. According to MD simulations, **4h**-enzyme reaches stability after 25 ns and **4h** showed binding interaction with both Cu^{2+} cofactor and His residues of the active site, therefore taking part in inhibition. The collective findings underscore the potential of kojic acid derivatives linked to amine pyridine in melanogenesis treatment, outperforming conventional kojic acid. This study enriches our understanding of the SARs and introduces compound **4h** as a candidate worthy of further exploration through animal and clinical studies. The implications of these discoveries extend to potential industrial applications within the realm of skincare and pharmaceuticals, aligning with the demand for effective solutions against abnormal pigmentation and its associated health risks.

4. Material and methods

4.1. Synthesis

Melting points were determined using a Kofler hot stage apparatus. IR spectra were recorded using KBr disks on a Bruker Tensor 27 FTIR spectrophotometer. The ^{1}H NMR and ^{13}C NMR spectra were recorded with a Bruker 500. Chemical shifts were reported at room temperature on a scale (ppm) with DMSO-d_6 as the solvents and *J* values are given in Hertz. All solvents and reagents were commercially available and used without further purification.

4.1.1. 3-Hydroxy-6-(hydroxymethyl)-2-(phenyl(pyridin-2-ylamino)methyl)-4H-pyran-4-one (4a)
Yield: 66 %; White powder. M.p. 188–190 °C. Rf = 0.32. IR (KBr) 3265, 1632, 1550, 1361, 1231 cm^{-1}; ^{1}H NMR (500 MHz, DMSO-d_6) δ 9.23 (s, 1H), 7.97 (d, *J* = 5.0 Hz, 1H), 7.54–7.17 (m, 7H), 6.71 (dd, *J* = 20.7, 8.6 Hz, 2H), 6.54 (t, *J* = 6.1 Hz, 1H), 6.31 (t, *J* = 1.1 Hz, 1H), 5.64 (t, *J* = 6.3 Hz, 1H), 4.29 (qd, *J* = 15.6, 6.0 Hz, 2H). ^{13}C NMR (125 MHz, DMSO-d_6) δ 174.2, 167.8, 157.8, 149.9, 147.8, 141.4, 140.5, 137.3, 128.9, 127.7, 127.23, 113.1, 109.5, 109.3, 59.9, 50.6. *Anal.* Calcd for C$_{18}$H$_{16}$N$_2$O$_4$: C 66.66, H 4.97, N 8.64; Found: C 66.46, H 5.16, N 8.52.

4.1.2. 2-((2-Fluorophenyl)(pyridin-2-ylamino)methyl)-3-hydroxy-6-(hydroxymethyl)-4H-pyran-4-one (4b)
Yield: 69 %; White powder. M.p. 194–196 °C. Rf = 0.28. IR (KBr) 3358, 1650, 1571, 1342, 1266, 1010 cm^{-1}; ^{1}H NMR (500 MHz, DMSO-d_6) δ 9.20 (s, 1H), 7.97 (d, *J* = 4.7 Hz, 1H), 7.54 (t, *J* = 8.0 Hz, 1H), 7.51–7.28 (m, 3H), 7.19 (q, *J* = 9.7, 8.3 Hz, 2H), 6.88 (d, *J* = 8.2 Hz, 1H), 6.71 (d, *J* = 8.4 Hz, 1H), 6.61–6.47 (m, 1H), 6.33 (s, 1H), 5.66 (d, *J* = 6.1 Hz, 1H), 4.27 (tt, *J* = 15.8, 9.0 Hz, 2H). ^{13}C NMR (125 MHz, DMSO-d_6) δ 174.2, 167.9, 161.2 ($^1J_{C\text{-}F}$ = 243.75 Hz), 157.5, 148.5, 147.8, 141.6, 137.3, 129.9 ($^3J_{C\text{-}F}$ = 8.75 Hz), 129.4 ($^4J_{C\text{-}F}$ = 3.75 Hz), 127.2 ($^3J_{C\text{-}F}$ = 13.75 Hz), 124.8 ($^4J_{C\text{-}F}$ = 3.75 Hz), 115.8 ($^2J_{C\text{-}F}$ = 21.25 Hz), 113.2, 109.5, 109.3, 59.9, 45.3. *Anal.* Calcd for C$_{18}$H$_{15}$FN$_2$O$_4$: C 63.16, H 4.42, N 8.18; Found: C 63.04, H 4.61, N 8.29.

4.1.3. 2-((3-Fluorophenyl)(pyridin-2-ylamino)methyl)-3-hydroxy-6-(hydroxymethyl)-4H-pyran-4-one (4c)
Yield: 76 %; White powder. M.p. 202–204 °C. Rf = 0.24. IR (KBr) 3250, 1656, 1580, 1356, 1250, 1000 cm^{-1}; ^{1}H NMR (500 MHz, DMSO-d_6) δ 9.35 (s, 1H), 7.98 (d, *J* = 5.1 Hz, 1H), 7.51–7.36 (m, 3H), 7.23 (dd, *J* = 12.7, 8.4 Hz, 2H), 7.11 (t, *J* = 8.7 Hz, 1H), 6.74 (t, *J* = 9.7 Hz, 2H), 6.57 (t, *J* = 6.2 Hz, 1H), 6.33 (s, 1H), 5.65 (s, 1H), 4.31 (tt, *J* = 16.3, 7.6 Hz, 2H). ^{13}C NMR (125 MHz, DMSO-d_6) δ 174.2, 167.9, 163.6 ($^1J_{C\text{-}F}$ = 242.5 Hz), 157.6, 149.3, 147.8, 143.6 ($^3J_{C\text{-}F}$ = 7.5 Hz), 141.5, 137.4, 130.9 ($^3J_{C\text{-}F}$ = 7.5 Hz), 123.3 ($^4J_{C\text{-}F}$ = 3.75 Hz), 114.7 ($^2J_{C\text{-}F}$ = 21.25 Hz), 113.9 ($^2J_{C\text{-}F}$ = 22.5 Hz), 113.4, 109.6, 109.4, 59.9, 50.2. *Anal.* Calcd for C$_{18}$H$_{15}$FN$_2$O$_4$: C 63.16, H 4.42, N 8.18; Found: C 63.01, H 4.55, N 8.22.

4.1.4. 2-((2-Chlorophenyl)(pyridin-2-ylamino)methyl)-3-hydroxy-6-(hydroxymethyl)-4H-pyran-4-one (4d)
Yield: 70 %; White powder. M.p. 196–198 °C. Rf = 0.28. IR (KBr) 3260, 1669, 1520, 1381, 1252, 799 cm^{-1}; ^{1}H NMR (500 MHz, DMSO-d_6) δ 9.18 (s, 1H), 7.94 (dd, *J* = 5.0, 1.8 Hz, 1H), 7.56 (dd, *J* = 7.4, 2.0 Hz, 1H), 7.51–7.19 (m, 6H), 6.82 (d, *J* = 7.8 Hz, 1H), 6.68 (d, *J* = 8.4 Hz, 1H), 6.53 (dd, *J* = 6.9, 5.2 Hz, 1H), 6.33 (s, 1H), 5.63 (t, *J* = 6.2 Hz, 1H), 4.22 (qd, *J* = 15.6, 5.2 Hz, 2H). ^{13}C NMR (125 MHz, DMSO-d_6) δ 174.3, 167.9, 157.5, 148.1, 147.8, 142.3, 137.6, 137.3, 133.0, 129.8, 129.5, 129.4, 127.6, 113.2, 109.4, 109.3, 59.8, 49.31. *Anal.* Calcd for C$_{18}$H$_{15}$ClN$_2$O$_4$: C 60.26, H.

4.1.5. 2-((3-Chlorophenyl)(pyridin-2-ylamino)methyl)-3-hydroxy-6-(hydroxymethyl)-4H-pyran-4-one (4e)
Yield: 80 %; White powder. M.p. 187–189 °C. Rf = 0.32. IR (KBr) 3265, 1658, 1380, 1241, 786 cm^{-1}; ^{1}H NMR (500 MHz, DMSO-d_6) δ 9.39 (s, 1H), 7.98 (dd, *J* = 5.1, 2.0 Hz, 1H), 7.59–7.22 (m, 6H), 6.74 (dd, *J* = 15.6, 8.5 Hz, 2H), 6.57 (dd, *J* = 7.1, 4.9 Hz, 1H), 6.34 (s, 1H), 5.67 (s, 1H), 4.31 (q, *J* = 15.5 Hz, 2H). ^{13}C NMR (125 MHz, DMSO-d_6) δ 174.2, 167.9, 157.6, 149.2, 147.8, 143.2, 141.5, 137.51, 133.6, 130.9, 127.8, 126.8, 125.9, 113.4, 109.6, 109.5, 59.9, 50.2. *Anal.* Calcd for C$_{18}$H$_{15}$ClN$_2$O$_4$: C 60.26, H 4.21, N 7.81; Found: C 60.04, H 4.35, N 7.64.

4.1.6. 2-((2-Bromophenyl)(pyridin-2-ylamino)methyl)-3-hydroxy-6-(hydroxymethyl)-4H-pyran-4-one (4f)
Yield: 68 %; White powder. M.p. 183–185 °C. Rf = 0.36. IR (KBr) 3255, 1671, 1580, 1350, 1248, 695 cm^{-1}; ^{1}H NMR (500 MHz, DMSO-d_6) δ 9.16 (s, 1H), 7.94 (dd, *J* = 4.9, 1.8 Hz, 1H), 7.65–7.57 (m, 1H), 7.53 (dd, *J* = 7.8, 1.7 Hz, 1H), 7.48–7.31 (m, 3H), 7.24 (td, *J* = 7.6, 1.7 Hz, 1H), 6.69 (dd, *J* = 21.4, 8.0 Hz, 2H), 6.53 (dd, *J* = 7.0, 5.1 Hz, 1H), 6.32 (s, 2H), 5.62 (t, *J* = 6.1 Hz, 1H), 4.25–4.15 (m, 2H). ^{13}C NMR (125 MHz, DMSO-d_6) δ 174.2, 167.9, 157.5, 148.2, 147.8, 142.5, 139.1, 137.2, 133.1, 129.8, 129.7, 128.1, 123.5, 113.1, 109.4, 109.3, 59.8, 51.8. *Anal.* Calcd for C$_{18}$H$_{15}$BrN$_2$O$_4$: C 53.62, H 3.75, N 6.95; Found: C 53.51, H 3.62, N 7.09.

4.1.7. 2-((3-Bromophenyl)(pyridin-2-ylamino)methyl)-3-hydroxy-6-(hydroxymethyl)-4H-pyran-4-one (4g)

Yield: 72 %; White powder. M.p. 200–202 °C. Rf = 0.32. IR (KBr) 3261, 1664, 1563, 1347, 1238, 700 cm^{-1}; ^{1}H NMR (500 MHz, DMSO-d_6) δ 9.37 (s, 1H), 7.97 (d, J = 5.1 Hz, 1H), 7.59 (s, 1H), 7.44 (dt, J = 25.6, 8.7 Hz, 3H), 7.38–7.27 (m, 1H), 6.72 (dd, J = 21.3, 8.5 Hz, 2H), 6.57 (t, J = 6.0 Hz, 1H), 6.32 (s, 1H), 5.65 (t, J = 6.3 Hz, 1H), 4.39–4.17 (m, 2H). ^{13}C NMR (125 MHz, DMSO-d_6) δ 174.2, 167.9, 157.5, 149.2, 147.81, 143.4, 141.4, 137.5, 131.2, 130.7, 129.6, 126.3, 122.2, 113.4, 109.6, 109.4, 59.9, 50.1. *Anal.* Calcd for C$_{18}$H$_{15}$BrN$_2$O$_4$: C 53.62, H 3.75, N 6.95; Found: C 53.47, H 3.91, N 6.83.

4.1.8. 3-Hydroxy-6-(hydroxymethyl)-2-((3-nitrophenyl)(pyridin-2-ylamino)methyl)-4H-pyran-4-one (4h)

Yield: 89 %; Light brown powder. M.p. 212–214 °C. Rf = 0.28. IR (KBr) 3250, 1653, 1552, 1351, 1234 cm^{-1}; ^{1}H NMR (500 MHz, DMSO-d_6) δ 9.49 (s, 1H), 8.26 (d, J = 2.0 Hz, 1H), 8.15 (dd, J = 8.2, 2.2 Hz, 1H), 7.97 (d, J = 5.0 Hz, 1H), 7.85 (d, J = 7.7 Hz, 1H), 7.75–7.55 (m, 2H), 7.54–7.41 (m, 1H), 6.80 (dd, J = 22.2, 8.4 Hz, 2H), 6.65–6.52 (m, 1H), 6.33 (s, 1H), 5.64 (t, J = 6.4 Hz, 1H), 4.29 (qd, J = 15.6, 4.9 Hz, 2H). ^{13}C NMR (125 MHz, DMSO-d_6) δ 174.2, 168.1, 157.4, 148.6, 148.4, 147.8, 143.1, 141.6, 137.6, 133.9, 130.6, 122.9, 121.5, 113.6, 109.7, 109.4, 59.8, 50.2. *Anal.* Calcd for C$_{18}$H$_{15}$N$_3$O$_6$: C 58.54, H 4.09, N 11.38; Found: C 58.28, H 4.17, N 11.22.

4.1.9. 3-Hydroxy-6-(hydroxymethyl)-2-((4-methoxy-3-nitrophenyl)(pyridin-2-ylamino)methyl)-4H-pyran-4-one (4i)

Yield: 89 %; Light brown powder. M.p. 216–218 °C. Rf = 0.26. IR (KBr) 3277, 1647, 1552, 1358, 1241 cm^{-1}; ^{1}H NMR (500 MHz, DMSO-d_6) δ 9.33 (s, 1H), 7.96 (d, J = 4.4 Hz, 1H), 7.89 (d, J = 4.7 Hz, 1H), 7.55 (d, J = 7.7 Hz, 1H), 7.49–7.36 (m, 2H), 7.12 (d, J = 7.6 Hz, 1H), 6.75 (dd, J = 28.7, 7.8 Hz, 2H), 6.55 (t, J = 6.4 Hz, 1H), 6.31 (s, 1H), 5.63 (t, J = 6.1 Hz, 1H), 4.28–4.19 (m, 2H), 3.78 (s, 3H).^{13}C NMR (125 MHz, DMSO-d_6) δ 174.1, 167.7, 157.8, 151.1, 149.4, 147.8, 141.4, 140.5, 137.3, 136.5, 131.6, 124.5, 114.9, 113.1, 109.4, 109.2, 59.8, 56.5, 50.6. *Anal.* Calcd for C$_{19}$H$_{17}$N$_3$O$_7$: C 57.14, H 4.29, N 10.52; Found: C 57.01, H 4.48, N 10.33.

4.1.10. 3-Hydroxy-6-(hydroxymethyl)-2-((pyridin-2-ylamino)(m-tolyl)methyl)-4H-pyran-4-one (4j)

Yield: 67 %; White powder. M.p. 203–205 °C. Rf = 0.24. IR (KBr) 3262, 1639, 1545, 1344, 1233 cm^{-1}; ^{1}H NMR (500 MHz, DMSO-d_6) δ 9.20 (s, 1H), 7.96 (d, J = 5.0 Hz, 1H), 7.49–7.36 (m, 1H), 7.31 (d, J = 8.7 Hz, 1H), 7.22 (d, J = 8.2 Hz, 3H), 7.12–7.02 (m, 1H), 6.69 (dd, J = 35.5, 8.5 Hz, 2H), 6.53 (t, J = 6.1 Hz, 1H), 6.31 (s, 1H), 5.64 (d, J = 6.3 Hz, 1H), 4.29 (qd, J = 15.5, 4.8 Hz, 2H), 2.28 (s, 3H). ^{13}C NMR (125 MHz, DMSO-d_6) δ 174.3, 167.9, 157.1, 149.8, 147.3, 140.3, 137.4, 132.9, 130.14, 128.8, 127.9, 127.5, 124.5, 113.3, 109.6, 109.5, 59.9, 50.4, 20.3. *Anal.* Calcd for C$_{19}$H$_{18}$N$_2$O$_4$: C 67.45, H 5.36, N 8.28; Found: C 67.36, H 5.53, N 8.17.

4.1.11. 3-Hydroxy-6-(hydroxymethyl)-2-((pyridin-2-ylamino)(p-tolyl)methyl)-4H-pyran-4-one (4k)

Yield: 69 %; White powder. M.p. 187–189 °C. Rf = 0.26. IR (KBr) 3251, 1625, 1539, 1382, 1243 cm^{-1}; ^{1}H NMR (500 MHz, DMSO-d_6) δ 9.30 (s, 1H), 7.95 (d, J = 5.2 Hz, 1H), 7.45 (t, J = 7.6 Hz, 1H), 7.35–7.32 (m, 1H), 7.27 (d, J = 7.6 Hz, 2H), 7.11 (d, J = 7.6 Hz, 2H), 6.68 (dd, J = 22.2, 8.4 Hz, 2H), 6.57 (t, J = 6.3 Hz, 1H), 6.33 (s, 1H), 5.63 (t, J = 6.1 Hz, 1H), 4.33–4.18 (m, 2H), 2.28 (s, 3H). ^{13}C NMR (125 MHz, DMSO-d_6) δ 174.2, 167.4, 157.6, 149.6, 147.5, 141.5, 140.0, 137.4, 136.5, 129.0, 126.9, 113.3, 109.8, 109.6, 59.8, 50.3, 20.7. *Anal.* Calcd for C$_{19}$H$_{18}$N$_2$O$_4$: C 67.45, H 5.36, N 8.28; Found: C 67.23, H 5.16, N 8.48.

4.1.12. 3-Hydroxy-2-((2-hydroxy-3-methoxyphenyl)(pyridin-2-ylamino)methyl)-6-(hydroxymethyl)-4H-pyran-4-one (4l)

Yield: 71 %; White powder. M.p. 183–185 °C. Rf = 0.20. IR (KBr) 3267, 1640, 1567, 1322, 1249, 1256 cm^{-1}; ^{1}H NMR (500 MHz, DMSO-d_6) δ 9.00 (s, 2H), 7.95 (d, J = 5.0 Hz, 1H), 7.40 (tt, J = 8.4, 1.7 Hz, 1H), 7.13 (d, J = 8.2 Hz, 1H), 6.95 (d, J = 7.7 Hz, 1H), 6.87 (d, J = 8.0 Hz, 1H), 6.74 (ddd, J = 9.7, 5.6, 1.4 Hz, 2H), 6.66 (d, J = 8.4 Hz, 1H), 6.52 (t, J = 6.1 Hz, 1H), 6.30 (s, 1H), 5.64 (t, J = 6.3 Hz, 1H), 4.37–4.12 (m, 2H), 3.78 (s, 3H). ^{13}C NMR (125 MHz, DMSO-d_6) δ 174.2, 167.5, 157.9, 150.0, 147.9, 147.5, 144.4, 141.6, 137.3, 126.7, 120.3, 119.0, 112.8, 111.3, 109.2, 109.2, 59.9, 56.2, 46.3. *Anal.* Calcd for C$_{19}$H$_{18}$N$_2$O$_6$: C 61.62, H 4.90, N 7.56; Found: C 61.51, H 5.09, N 7.34.

4.1.13. 3-Hydroxy-6-(hydroxymethyl)-2-((4-(phenoxymethyl)phenyl)(pyridin-2-ylamino)methyl)-4H-pyran-4-one (4m)

Yield: 85 %; White powder. M.p. 168–170 °C. Rf = 0.24. IR (KBr) 3264, 1647, 1535, 1386, 1251 cm^{-1}; ^{1}H NMR (500 MHz, DMSO-d_6) δ 9.16 (s, 1H), 7.95 (d, J = 5.0 Hz, 1H), 7.45–7.35 (m, 5H), 7.32 (dd, J = 7.7, 5.0 Hz, 3H), 7.26 (d, J = 8.6 Hz, 1H), 7.03–6.94 (m, 2H), 6.70 (d, J = 8.4 Hz, 1H), 6.58 (d, J = 8.6 Hz, 1H), 6.53 (t, J = 6.1 Hz, 1H), 6.29 (s, 1H), 5.62 (t, J = 6.3 Hz, 1H), 5.07 (s, 2H), 4.27 (dq, J = 15.8, 7.7, 6.7 Hz, 2H). ^{13}C NMR (125 MHz, DMSO-d_6) δ 174.1, 167.7, 157.2, 155.9, 149.2, 147.5, 140.8, 137.8, 136.5, 134.5, 128.2, 127.2, 126.4, 125.1, 114.9, 113.1, 109.4, 109.0, 69.4, 59.5, 50.4. *Anal.* Calcd for C$_{25}$H$_{22}$N$_2$O$_5$: C 69.76, H 5.15, N 6.51; Found: C 69.55, H 5.27, N 6.44.

4.2. Tyrosinase inhibitory assay

To evaluate tyrosinase inhibition of synthesized compounds, the assay was performed as described previously [,34]. The reaction was started by loading 160 μl of phosphate buffer (20 mM, pH 6.8), 10 μl of mushroom tyrosinase (500 U/ml), and 10 μl of test derivatives at different concentrations in a 96-well plate. After 20 min incubation at room temperature, 20 μl (0.5 mM) L-DOPA (3, 4-dihydroxyphenylalanine) was added and the absorbance was determined as a measure of dopachrome formation by a plate reader at 475 nm. Kojic acid was used as a standard inhibitor for reference. For clear statistical analysis, experiments were performed three times in duplet. First, percentage inhibition was determined and then IC$_{50}$ was calculated using curve expert, and the results were compared with standard inhibitor.

4.3. Enzyme kinetic studies

The mode of inhibition of the most active compound 3-hydroxy-6-(hydroxymethyl)-2-((3-nitrophenyl)(pyridin-2-ylamino)methyl)-4*H*-pyran-4-one identified with the lowest IC_{50}, was investigated against tyrosinase activity at different concentrations of L-DOPA (0, 0.5, 0.75, 1, 1.5 mM) as substrate in the absence and presence of 3-hydroxy-6-(hydroxymethyl)-2-((3-nitrophenyl)(pyridin-2-ylamino) methyl)-4H-pyran-4-one at different concentrations (5, 10, 20, 40 and 80 μM). A Lineweaver–Burk plot was generated to identify the type of inhibition and the Michaelis–Menten constant (K_m) value was determined from the plot between the reciprocal of the substrate concentration (1/[S]) and reciprocal of enzyme rate (1/V) over various inhibitor concentrations [13].

4.4. Molecular docking

The molecular docking studies were performed using the Maestro Molecular Modeling platform (version 10.5) by Schrödinger, LLC. The X-ray crystal structure of the receptor (PDB ID: 2Y9X) was extracted from the PDB database. The protein is then prepared using a protein preparation wizard, the co-crystallized ligands and all water molecules were removed, the missing side chains and loops were filled using the prime tool, and PROPKA assigned H-bonds at pH: 7.4. To prepare the ligands, the 2D structures of the ligands were drawn in ChemDraw and converted into SDF files and subjected to ligprep module. Ligands were prepared by OPLS_2005 force field using EPIK. The grid box was generated for each binding site using entries with a box size of 20 Å. The derivative was docked on binding sites using induced-fit docking, reporting 10 poses per ligand to form the final complex.

4.5. Molecular dynamic simulation

The molecular simulation was performed using the Desmond v5.3 (Schrödinger 2018-4 suite). To build the system for MD simulation, the protein-ligand complexes were solvated with SPC explicit water molecules and placed in the center of an orthorhombic box of appropriate size in the periodic boundary condition. Sufficient counter-ions and a 0.15 M solution of NaCl were also utilized to neutralize the system and simulate the real cellular ionic concentrations. The MD protocol involved minimization, pre-production, and finally production MD simulation steps. The minimization procedure allowed the entire system to relax for 2500 steps by the steepest descent approach. Then the system's temperature was raised from 0 to 300 K with a small force constant on the enzyme to restrict any drastic changes. MD simulations were performed via NPT (constant number of atoms, constant pressure i.e. 1.01325 bar, and constant temperature i.e. 300 K) ensemble. The Nose-Hoover chain method was used as the default thermostat with 1.0 ps interval and Martyna-Tobias-Klein as the default barostat with 2.0 ps interval by applying isotropic coupling style. Long-range electrostatic forces were calculated based on the particle-mesh-based Ewald approach with the cut-off radius for Columbia forces set to 9.0 Å. Finally, the system was subjected to produce MD simulations for 30 ns for each protein-ligand complex. The systems' dynamic behavior and structural changes were analyzed by calculating the RMSD and RMSF [35].

Funding

CRediT authorship contribution statement

Davood Rezapour Niri: Investigation, Methodology, Validation. **Mohammad Hosein Sayahi:** Data curation, Formal analysis, Investigation, Methodology. **Somayeh Behrouz:** Data curation, Formal analysis, Investigation, Methodology. **Ali Moazzam:** Data curation, Formal analysis, Methodology, Software, Writing – original draft. **Fatemeh Rasekh:** Formal analysis, Investigation, Methodology, Resources, Software. **Nader Tanideh:** Data curation, Investigation, Methodology, Validation. **Cambyz Irajie:** Data curation, Investigation, Methodology, Software, Writing – original draft. **Mohammad Seif Nezhad:** Data curation, Formal analysis, Investigation, Methodology. **Bagher Larijani:** Investigation, Methodology, Validation, Visualization. **Aida Iraji:** Conceptualization, Data curation, Investigation, Methodology, Writing – original draft, Writing – review & editing. **Mohammad Mahdavi:** Conceptualization, Supervision, Validation, Visualization, Writing – review & editing.

Declaration of competing interest

The authors declare that they have no known competing financial interests or personal relationships that could have appeared to influence the work reported in this paper.

Appendix A. Supplementary data

Supplementary data to this article can be found online at https://doi.org/10.1016/j.heliyon.2023.e22009.

References

[1] M. Hajimiri, et al., Rational design, synthesis, in vitro, and in silico studies of chlorophenylquinazolin-4 (3H)-One containing different aryl acetohydrazides as tyrosinase inhibitors, Chem. Biodivers. (2022), e202100964.

[2] R.J. Obaid, et al., Natural and synthetic flavonoid derivatives as new potential tyrosinase inhibitors: a systematic review, RSC Adv. 11 (36) (2021) 22159–22198.

[3] N. Alizadeh, et al., Evaluating the effects of disubstituted 3-hydroxy-1H-pyrrol-2 (5H)-one analog as novel tyrosinase inhibitors, Bioorg. Chem. 126 (2022), 105876.

[4] H. Hosseinpoor, et al., Anti-melanogenesis and anti-tyrosinase properties of aryl-substituted acetamides of phenoxy methyl triazole conjugated with thiosemicarbazide: design, synthesis and biological evaluations, Bioorg. Chem. 114 (2021) 104979.

[5] A. Iraji, et al., Design, synthesis, in vitro and in silico studies of novel Schiff base derivatives of 2-hydroxy-4-methoxybenzamide as tyrosinase inhibitors, Drug Dev. Res. 82 (4) (2021) 533–542.

[6] W.-M. Chai, et al., Condensed tannins from longan bark as inhibitor of tyrosinase: structure, activity, and mechanism, J. Agric. Food Chem. 66 (4) (2018) 908–917.

[7] S. Xue, et al., Design, synthesis, and biological evaluation of novel hybrids containing dihydrochalcone as tyrosinase inhibitors to treat skin hyperpigmentation, J. Med. Chem. 66 (7) (2023) 5099–5117.

[8] H. Raza, et al., 2-Aminothiazole-Oxadiazole bearing N-arylated butanamides: convergent synthesis, tyrosinase inhibition, kinetics, structure-activity relationship, and binding conformations, Chem. Biodivers. 20 (2) (2023), e202201019.

[9] J. Lee, et al., Design and synthesis of (Z)-2-(Benzylamino)-5-benzylidenethiazol-4 (5 H)-one derivatives as tyrosinase inhibitors and their anti-melanogenic and antioxidant effects, Molecules 28 (2) (2023) 848.

[10] M. Noori, et al., Thioquinoline derivatives conjugated to thiosemicarbazide as potent tyrosinase inhibitors with anti-melanogenesis properties, Sci. Rep. 13 (1) (2023) 2578.

[11] Z. Najafi, et al., Design, synthesis, in vitro, and in silico studies of novel benzylidene 6-methoxy-1-tetralone linked to benzyloxy and benzyl -1,2,3- triazole rings as potential tyrosinase inhibitors, J. Mol. Struct. 1271 (2023), 134018.

[12] M.M. Al-Rooqi, et al., Evaluation of 2,3-Dihydro-1,5-benzothiazepine derivatives as potential tyrosinase inhibitors: in vitro and in silico studies, ACS Omega 8 (19) (2023) 17195–17208.

[13] J. Ashraf, et al., Structure-based designing and synthesis of 2-phenylchromone derivatives as potent tyrosinase inhibitors: in vitro and in silico studies, Bioorg. Med. Chem. 35 (2021) 116057.

[14] J. Ashraf, et al., Exploring 3-hydroxyflavone scaffolds as mushroom tyrosinase inhibitors: synthesis, X-ray crystallography, antimicrobial, fluorescence behaviour, structure-activity relationship and molecular modelling studies, J. Biomol. Struct. Dyn. 39 (18) (2021) 7107–7122.

[15] R.I. Alsantali, et al., Flavone-based hydrazones as new tyrosinase inhibitors: synthetic imines with emerging biological potential, SAR, molecular docking and drug-likeness studies, J. Mol. Struct. 1251 (2022), 131933.

[16] E.U. Mughal, et al., Design, synthesis, and structural characterization of thioflavones and thioflavonols as potential tyrosinase inhibitors: in vitro and in silico studies, ACS Omega 7 (20) (2022) 17444–17461.

[17] N.A. Alshaye, et al., Synthesis and biological evaluation of substituted aurone derivatives as potential tyrosinase inhibitors: in vitro, kinetic, QSAR, docking and drug-likeness studies, J. Biomol. Struct. Dyn. (2022) 1–16.

[18] Y. Song, et al., The hypopigmentation mechanism of tyrosinase inhibitory peptides derived from food proteins: an overview, Molecules 27 (9) (2022) 2710.

[19] M. Ashooriha, et al., Kojic acid–natural product conjugates as mushroom tyrosinase inhibitors, Eur. J. Med. Chem. 201 (2020), 112480.

[20] M. Ashooriha, et al., Application of kojic acid scaffold in the design of non-tyrosinase enzyme inhibitors, Chem. Biol. Drug Des. 100 (2) (2022) 290–303.

[21] V. Phasha, et al., Review on the use of kojic acid—a skin-lightning ingredient, Cosmetics 9 (3) (2022) 64.

[22] Y.S. Lee, et al., Synthesis of tyrosinase inhibitory kojic acid derivative, Arch. Pharmazie 339 (3) (2006) 111–114.

[23] N. Sepehri, et al., The natural-based optimization of kojic acid conjugated to different thio-quinazolinones as potential anti-melanogenesis agents with tyrosinase inhibitory activity, Bioorg. Med. Chem. 36 (2021), 116044.

[24] M. El-Naggar, et al., Pyridine-ureas as potential anticancer agents: synthesis and in vitro biological evaluation, Molecules 23 (6) (2018) 1459.

[25] M. Helal, et al., Synthesis, biological evaluation and molecular modeling of novel series of pyridine derivatives as anticancer, anti-inflammatory and analgesic agents, Spectrochim. Acta Mol. Biomol. Spectrosc. 135 (2015) 764–773.

[26] S. Eryılmaz, et al., Derivatives of pyridine and thiazole hybrid: synthesis, DFT, biological evaluation via antimicrobial and DNA cleavage activity, Bioorg. Chem. 95 (2020), 103476.

[27] T.B. Tafesse, et al., Synthesis and biological evaluation of 2-(2-methyl-1H-pyrrol-3-yl)-2-oxo-N-(pyridine-3-yl) acetamide derivatives: in vitro α-glucosidase inhibition, and kinetic and molecular docking study, Chem. Pap. 74 (5) (2020) 1583–1596.

[28] J. Sim, et al., Inhibitory effect of chlorogenic acid analogues comprising pyridine and pyrimidine on α-MSH-stimulated melanogenesis and stability of acyl analogues in methanol, Pharmaceuticals 14 (11) (2021) 1176.

[29] T. Pillaiyar, et al., Inhibitors of melanogenesis: an updated review, J. Med. Chem. 61 (17) (2018) 7395–7418.

[30] H. Jo, et al., Synthesis and biological evaluation of caffeic acid derivatives as potent inhibitors of α-MSH-stimulated melanogenesis, Bioorg. Med. Chem. Lett 27 (15) (2017) 3374–3377.

[31] M. Michalak, Plant-Derived antioxidants: significance in skin health and the ageing process, Int. J. Mol. Sci. 23 (2) (2022).

[32] A. Ullah, S. Munir, Important flavonoids and their role as a therapeutic agent 25 (22) (2020).

[33] M. Michalak, Plant-derived antioxidants: significance in skin health and the ageing process, Int. J. Mol. Sci. 23 (2) (2022) 585.

[34] A. Iraji, et al., Synthesis, biological evaluation and molecular docking analysis of vaniline–benzylidenehydrazine hybrids as potent tyrosinase inhibitors, BMC chemistry 14 (1) (2020) 1–11.

[35] A. Iraji, et al., Design, synthesis, spectroscopic characterization, in vitro tyrosinase inhibition, antioxidant evaluation, in silico and kinetic studies of substituted indole-carbohydrazides, Bioorg. Chem. 129 (2022), 106140.